Journal of Pain 39 (2026) 105594

Contents lists available at ScienceDirect

The Journal of Pain

journal homepage: www.jpain.org

Original reports

Post-traumatic osteoarthritis in aged rodents is associated with brain changes that correlate with joint remodeling

Jacob L. Griffith [a], Pedro A. Valdes-Hernandez [b,c], Taylor D. Yeater [a], Shane H. Priester [a], Marcelo Febo [d], Yenisel Cruz-Almeida [b,c,d], Kyle D. Allen [a,b,d,e,*,a]

[a] J. Crayton Pruitt Family Department of Biomedical Engineering, University of Florida, Gainesville, FL, USA
[b] Pain Research and Intervention Center of Excellence, University of Florida, Gainesville, FL, USA
[c] Department of Community Dentistry and Behavioral Science, University of Florida, Gainesville, FL, USA
[d] McKnight Brain Institute, University of Florida, Gainesville, FL, USA
[e] Department of Orthopedics and Rehabilitation, College of Medicine, University of Florida, Gainesville, FL, USA

ARTICLE INFO

Keywords:
Osteoarthritis
Brain
MRI
Tactile sensitivity
Aging
Rat animal model
Joint histology

ABSTRACT

Preclinical models of osteoarthritis (OA) can provide insights into joint-level remodeling and pain-related behaviors, but effects beyond the joint are poorly understood. The current study investigates joint remodeling and brain remodeling using aged rats in a surgical rodent model of post-traumatic OA. Male and female Fischer 344 rats (68 weeks old) received either a skin incision (n=6 male and n=10 female) or medial collateral ligament transection plus medial meniscus transection (MCLT+MMT) surgery (n=5 male and n=11 female). Tactile sensitivity was assessed pre-surgery and 4-, 8-, 12-, and 16-weeks post-surgery. Neuroimaging was performed pre-surgery and 6- and 14-weeks post-surgery, with analyses focused on gray matter volume, blood oxygen level dependent (BOLD) signal, and functional connectivity. Following euthanasia, histological analysis was performed to assess joint changes. Histology confirmed advanced cartilage loss and bone damage in animals with MCLT+MMT animals relative to skin-incision sham; however, tactile sensitivity decreased over time for both surgery groups. From the neuroimaging data, differences between the MCLT+MMT and skin-incision groups were present for both males and females at week 6 and week 14. Differences include gray matter volume, BOLD signal, and functional connectivity in regions responsible for pain transmission and modulation (thalamus, somatosensory cortex, and periaqueductal gray), along with the emotional and affective aspects of pain (striatum, hippocampus, prefrontal cortex, and amygdala). Despite a lack of differences in tactile sensitivity between groups, these findings in the central circuits involved in sensory and nociceptive processing indicate an association with knee OA development and brain remodeling.
Perspective: This work is the first to examine brain remodeling in the acute and chronic stages of osteoarthritis pain using the medial meniscus transection model in aged animals. Results demonstrate evidence of brain remodeling in a preclinical model of osteoarthritis and help elucidate osteoarthritis effects beyond the joint.

Introduction

Osteoarthritis (OA) is a painful and debilitating disease involving effects within and beyond the joint. While once considered a "wear and tear" disease centered on cartilage degradation, OA pathogenesis is now understood to involve chronic low-grade inflammation altering the entire joint. However, the relationship between joint remodeling and pain-related symptoms is poorly understood. Symptomatic presentation of chronic joint pain in OA may involve local and systemic factors, where recent work highlights potential impacts of OA beyond the joint including autonomic dysfunction,[1–4] central sensitization, impaired descending inhibitory control, and brain remodeling.[5–10]

In the limited existing literature, preclinical models have focused on functional brain changes in pain transmission and modulation,[8,11] including sex- and age-related differences in the pain modulatory network.[8] OA involves the combination of both nociceptive and

* Correspondence to: J. Crayton Pruitt Family Department of Biomedical Engineering, University of Florida, 1275 Center Drive, Biomedical Sciences Building, Gainesville, Florida 32610, USA.
E-mail address: kyle.allen@bme.ufl.edu (K.D. Allen).
[a] (352) 273–9337

https://doi.org/10.1016/j.jpain.2025.105594
Received 16 April 2025; Received in revised form 10 October 2025; Accepted 3 November 2025
Available online 22 November 2025

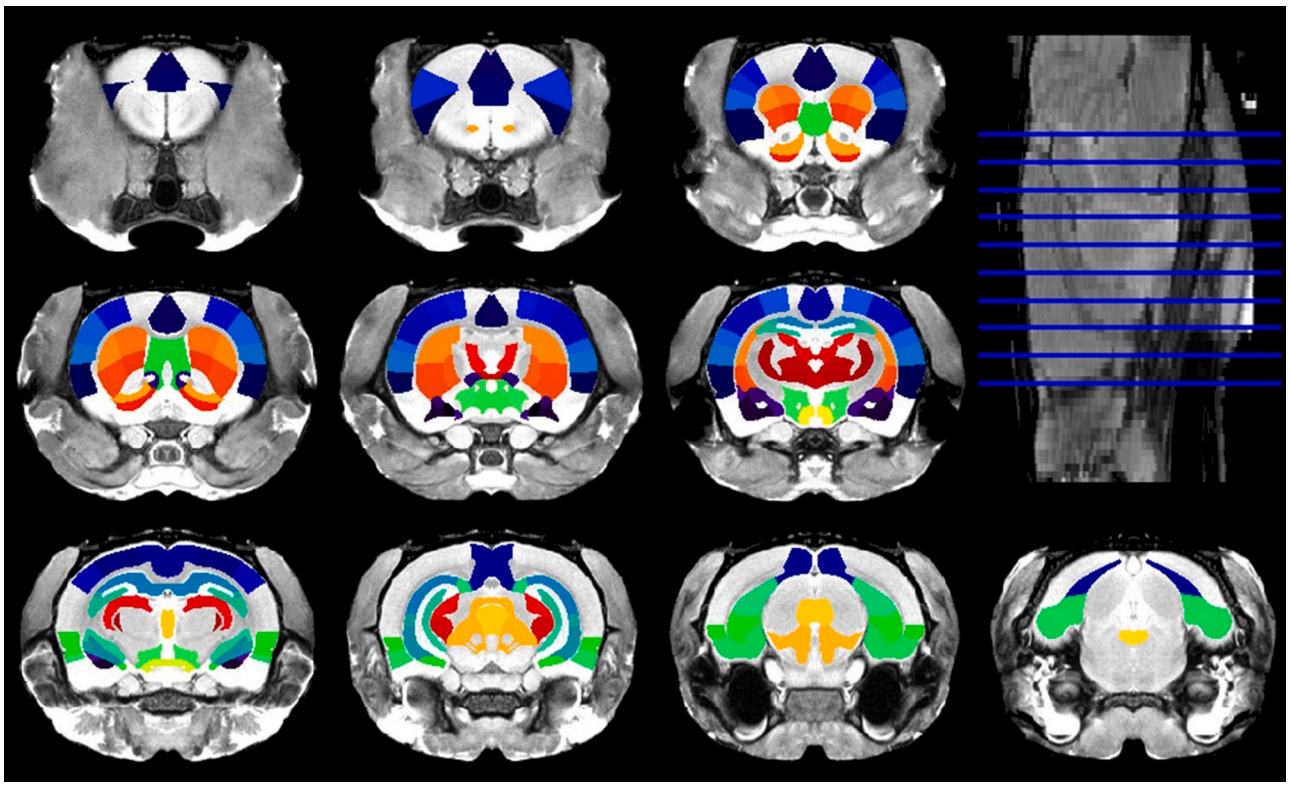

Fig. 1. Visual representation of pain-processing regions within the brain.

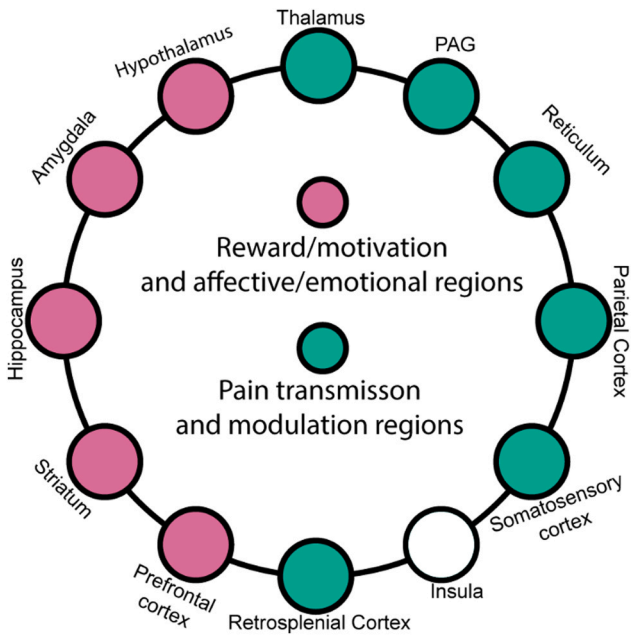

Fig. 2. MRI analyses focused on regions implicated in pain transmission and modulation (green) and the emotional/affective aspect of pain and reward/motivation (magenta). The insula is labeled in white as the posterior insula is primarily associated with the sensory-discriminative aspects of nociception, whereas the anterior insula is linked to the emotional-affective components of the pain experience.

neuropathic pain.[12,13] In humans, chronic pain from the periphery — whether nociceptive, neuropathic, or a combination of sources — chronic pain disrupts the brain's emotional and reward systems,[14,15] particularly the nucleus accumbens (NAc) and medial prefrontal cortex (mPFC), leading to altered responses to rewards and emotions.[16–18] This occurs because chronic pain can shift brain processing from sensory regions to emotional circuits, creating maladaptive connections between pain and reward-motivational pathways. Despite this well-established understanding in human studies, the existing preclinical literature has significant gaps. Few animal models have systematically examined functional brain changes in pain transmission and modulation,[8] including important sex- and age-related differences in pain modulatory networks with fewer studies in OA. However, these broader OA-related brain changes — particularly those affecting emotional and motivational circuits beyond pain transmission pathways — have not been well characterized in preclinical OA models.

Guided by existing clinical and preclinical neuroimaging studies in OA, we hypothesized that, in a surgical model of knee OA, widespread structural and functional remodeling would occur in regions associated with both sensory processing, discrimination, and pain modulation as well as in regions involved with the emotional and affective aspects of pain. This was assessed through longitudinal anatomical and functional magnetic resonance imaging (MRI) using a rat knee OA model in aged male and female rats. To provide context to the neuroimaging results, we also evaluated the development of OA-related joint remodeling and symptoms. The longitudinal nature of this study combined with the use of aged male and female animals provides a new perspective on disease progression and brain structure and function at different stages of disease, including time points previously reflective of symptomatic onset and sustained symptoms (pain chronification).

Materials and methods

Experimental design

To assess our hypothesis, this study included longitudinal evaluation of magnetic resonance imaging (MRI) of the rat brain. This study used three cohorts of male and female Fischer 344 rats with surgical induction of knee OA through a medial collateral ligament transection

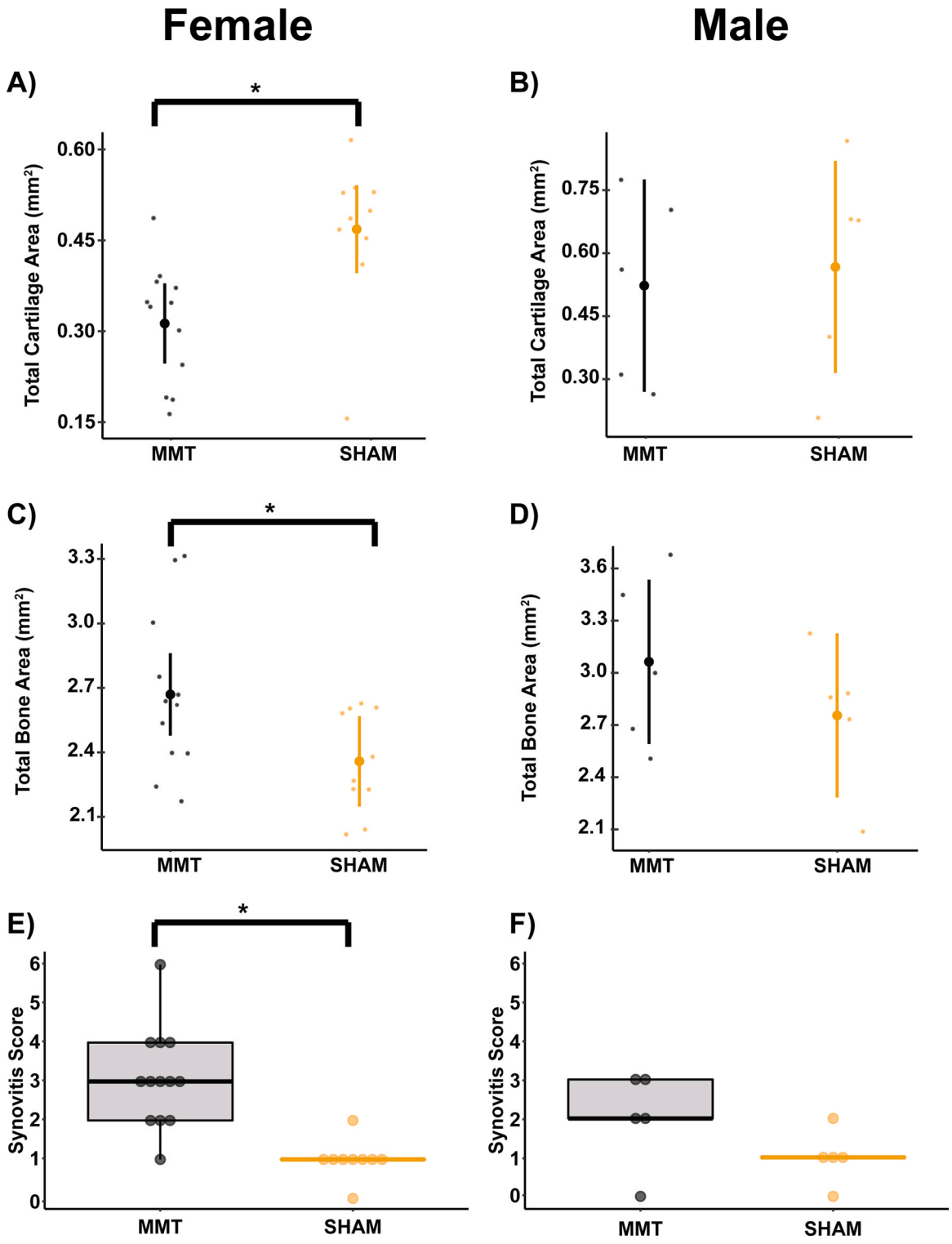

Fig. 3. Quantitative analysis of joint histology showed differences for females showed differences in **A)** cartilage area, **C)** subchondral bone area, and **E)** synovitis score. For males, there was no differences for **B)** cartilage area, **D)** subchondral bone area, and **F)** synovitis score.

followed by a medial meniscus transection (MCLT+MMT) surgery. Skin-incision was used as a sham control. Animals were randomly assigned into groups using a random number generator and all surgeries and data collections were performed via experimenters blinded to the group. To test our hypotheses independently in males and females, *apriori* power estimates identified the target number of animals per group as n=10 per sex for both the MCLT+MMT and skin-incision sham groups. Anticipating dropout with the use of aged animals, we began the study with 29 females and 28 males. However, 8 male rats and 1 female rat were removed from the study as a humane endpoint due to gastrointestinal distress related to meloxicam, and 9 male rats and 7 female rats were removed from the study as a humane endpoint due to age-related health concerns – most commonly age-related leukemia, which is highly prevalent in aged Fischer rats. In the end, final numbers for groups are n=5 male MCLT+MMT, n=6 male skin-incision, n=11 female MCLT+MMT, and n=10 female skin-incision, falling short of our target

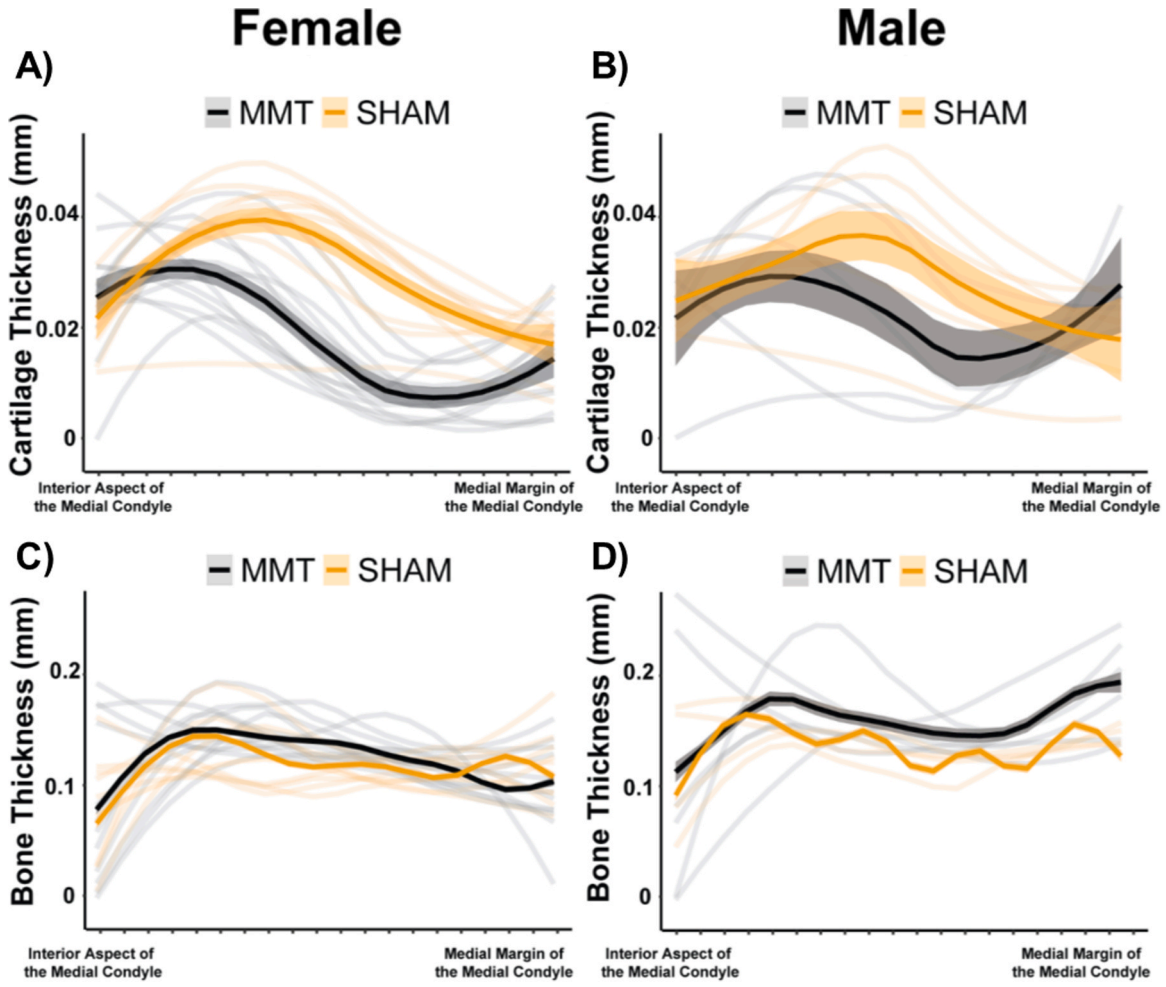

Fig. 4. Location dependent cartilage changes were observed for both females and males and location dependent subchondral bone changes were observed for females and males.

of n=10 per sex for the male cohort. At 6 weeks and 14 weeks after surgery, assessments of tactile allodynia and magnetic resonance imaging of the brain were conducted. The 6 week timepoint aligned with prior reports of symptomatic onset in the MCLT+MMT model (though these data were collected at young ages[19] or middle age animals[20]); the second time point was selected to reflect sustained symptoms.

Animals

Fischer 344 rats (68 weeks of age) were obtained from the National Institute on Aging aged rodent colony and acclimated for at least five days at the University of Florida (UF) animal care facilities. For the female animals, the mean weight at surgery was 243 g with a range from 202 to 275 g. Whereas, for males, the mean weight at surgery was 409 g with a range from 348 g to 480 g. Animals were housed two per cage in a reverse light cycle environment (12-hour light/dark cycle with the dark cycle occurring during the day) with access to food and water ad libitum. In the case of animal dropout, the cage partner remained solo and environmental enrichment toys were added. Standard bedding and housing were used. All procedures were approved by the UF Institutional Animal Care and Use Committee.

Surgical induction of knee osteoarthritis

This study used medial collateral ligament transection followed by a medial meniscus transection (MCLT+MMT) for the surgical induction of knee OA. Rats were first anesthetized with isoflurane (2% in oxygen). Then, right knees were prepared for surgery by shaving the area and applying 3 rounds of betadine and 70% ethanol washes, ending with a fourth application of betadine. For all surgeries, a 2–3 cm incision was made along the medial portion of the right hind limb. Skin-incision shams were closed following this incision. For the MCLT+MMT group, the MCL was visualized and transected, followed by the joint being placed in a valgus orientation to allow for transection of the medial meniscus in its neutral position. Muscle and skin were closed using sterile 4–0 absorbable sutures. Surgeons were blinded to the animal group until the point of deviation of the surgery.

Tactile sensitivity

Tactile sensitivity was measured at baseline and every 4 weeks across 16 weeks post-surgery. Prior to baseline testing, animals were acclimated to the tactile sensitivity testing environment three times for 30 min each. During testing, a series of von Frey filaments (Stoelting Co., Wood Dale, IL – item 58011) were applied to the plantar region of the hindfoot using Chaplan's up-down approach.[21] Following testing, 50% withdrawal thresholds were then approximated using Chaplan's estimations.

MRI data collection

All MRI scans consisted of a T2 weighted structural MRI and resting state functional MRI (rs-fMRI) collected using an 11.1 T Bruker AV3 HD scanner MRI system (Magnex Scientific). The system is a Bruker AV3 HD

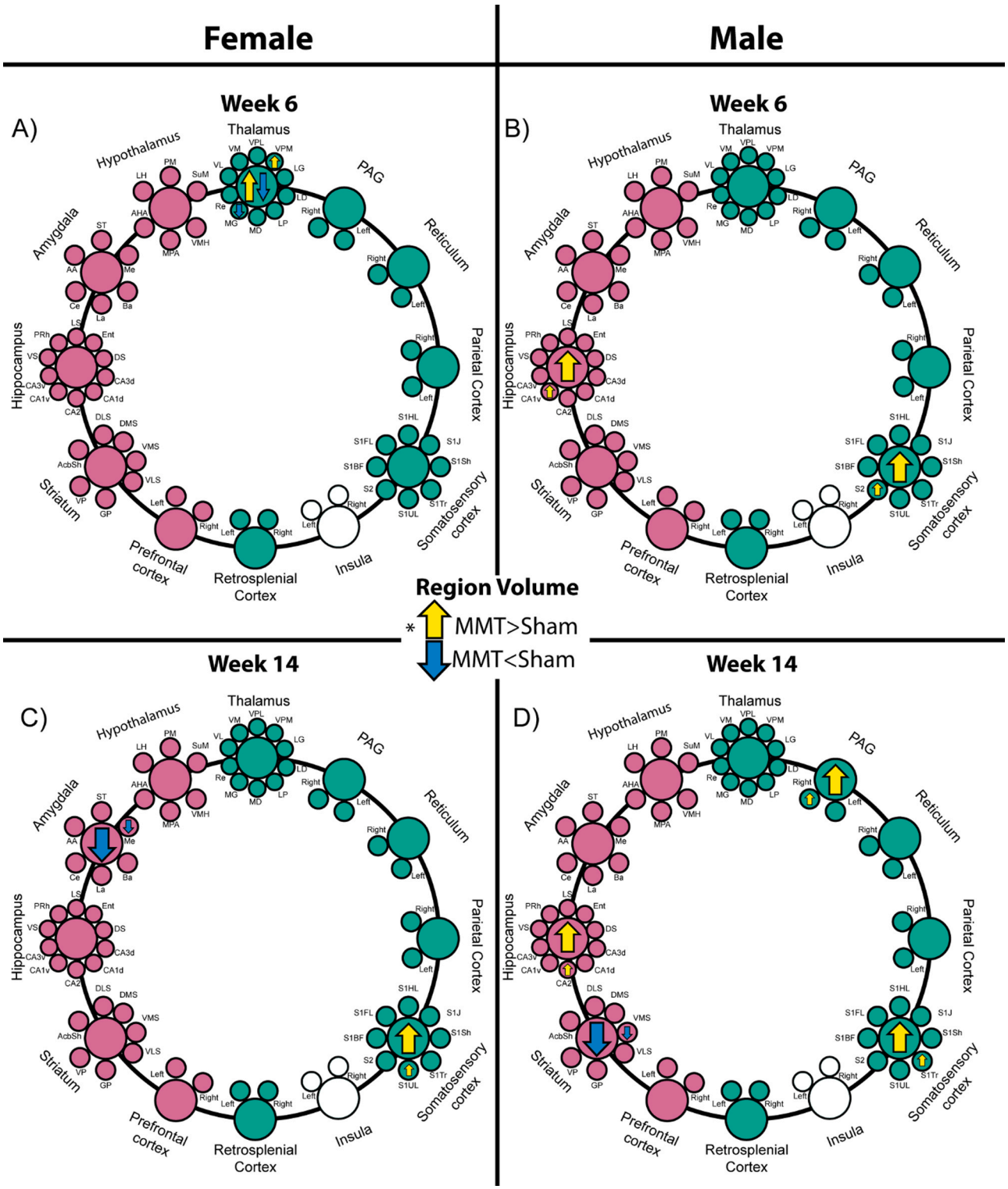

Fig. 5. Group differences in gray matter volume are shown for females at week 6 **(A)** and week 14 **(C)** and males at week 6 **(B)** and week 14 **(D)**. Higher regional volumes of the MCLT+MMT group relative to skin-incision sham is indicated using a yellow arrow and lower volumes are shown with a blue arrow. Regions in magenta are related to the emotional/affective aspects of pain whereas green regions are associated with sensory discrimination. Statistical significance was determined following the Benjamini-Hochberg correction ($p_{adj} < 0.05$).

console/Paravision 6.01 with custom-made 2.5 cm × 3.5 cm quadrature radiofrequency (RF) surface transmit/receive coil tuned to 470.7 MHz (^{1}H resonance) (RF engineering lab, Advanced Magnetic Resonance Imaging and Spectroscopy Facility, Gainesville, FL). For resting state functional MRI (rs-fMRI), a single-shot spin-echo echo planar imaging (SE-EPI) sequence was acquired with the following acquisition parameters: echo time (TE) 15 ms; repetition time (TR) 2 s; 450 repetitions for a total acquisition time of 15 min; field of view (FOV) 24 mm x 18 mm; 25 slices 0.9 mm thick; and data matrix 64 rows × 48 columns. The in-plane resolution was 0.375 × 0.375 mm, which is within the range of geometric parameters of most rat fMRI studies. Also, rs-fMRI was collected with reversed phase-encode blips, resulting in pairs of

Table 1
Statistically significant group differences in gray matter volume, including effect size and p-values before and after false discovery rate correction.

	Mean [95% confidence interval]				
	MCLT+MMT	Skin-incision	η^2	p_{raw}	p_{adj}
Volume comparison at week 6 (male)					
Secondary somatosensory cortex (right)	0.407 [-0.013, 0.826]	-0.623 [-0.921, −0.325]	0.28	0.00015	0.00925
Ventral CA1 of hippocampus (right)	1.75 [0.932, 2.57]	-0.138 [-0.719, 0.443]	0.25	0.00033	0.01993
Volume comparison at week 14 (male)					
Central gray (right)	0.394 [0.147, 0.642]	-0.446 [-0.691, −0.201]	0.37	$5.5*10^{-6}$	0.00033
Somatosensory cortex trunk (left)	0.577 [-0.034, 1.19]	-1.38 [-1.99, −0.779]	0.33	$2.5*10^{-5}$	0.00148
CA2 of hippocampus (right)	0.15 [-0.027, 0.328]	-0.352 [-0.527, −0.177]	0.13	0.0002	0.0118
Ventromedial striatum (left)	-1.11 [-1.98, −0.234]	0.799 [-0.067, 1.66]	0.23	69	0.04166
Volume comparison at week 6 (female)					
Ventral posteriomedial nucleus of the thalamus (right)	0.567 [0.294, 0.839]	-0.262 [-0.587, 0.064]	0.2	0.00017	0.01046
Medial geniculate of thalamus (right)	-0.341 [-0.583, −0.098]	0.390 [0.099, 0.680]	0.19	0.0002	0.01202
Volume comparison at week 14 (female)					
Somatosensory cortex upper lip (left)	0.848 [0.194, 1.50]	-1.08 [-1.82, −0.341]	0.2	0.00019	0.01168
Medial nucleus of the amygdala (right)	-0.312 [-0.480, −0.143]	0.144 [-0.046, 0.334]	0.17	0.00055	0.03291

images with distortions going in opposite directions. From these pairs the susceptibility-induced off-resonance field was estimated using a method similar to that described in[22] as implemented in FSL[23] and the two images were combined into a single corrected one. Anatomic scans were collected using a fast spin-echo sequence (Turbo RARE) with the following parameters: TR/TE_{eff} 5052.2/37.35 ms; RARE (rapid acquisition with relaxation enhancement) factor 16; number of averages 14; FOV 24 × 18 mm; 25 slices 36 mm thick; and data matrix 256 × 192, resulting in a resolution of 93.75 × 93.75 × 900 μm. During the scans, rats were under 1.5–1.8% isoflurane gas anesthesia delivered at 2 L/min in oxygen. Spontaneous breathing rates were continuously monitored throughout the scan and core body temperature was maintained using a water recirculation system. Due to dropout, 56 animals were scanned at baseline, 33 animals at week 6, and 32 animals at week 14. The week 6 and week 14 timepoints were chosen based on our previous work.[19,20]

MRI preprocessing and analysis

Following scan acquisition, preprocessing and analysis were performed to evaluate changes in region volume, blood oxygenation level dependent (BOLD) signal, and region to region functional connectivity. Structural MRIs were corrected for coil-related intensity inhomogeneities using N4[24] and nonlinearly spatially registered to the Ferris brain space[25] using FSL[26] and ANTS.[27] This transformation was used to warp an atlas of brain structures to the individual space, for which volumes were calculated as the integral of brain tissue probability (gray or white matter) within the structure, obtained using.[28] Rs-fMRIs were skull stripped, de-spiked and slice timed using AFNI, unwarped using FSL's top-up, motion corrected using FSL temporally band-pass (0.01–0.12 Hz) filtered and denoised using MELODIC.[23] The BOLD signal in each region was calculated as the average of the BOLD time series data within an ellipsoid expanding 0.5 mm mediolaterally, 0.5 mm ventrodorsally, and 5 mm rostrocaudally from the center of the region. Resting-state functional connectivity (rs-FC) between every pair of structures in the atlas was calculated by taking the Fisher-transformed Pearson correlation of the time series of the BOLD signal. Analysis in this study focused on pain-processing regions, illustrated in Figure 1.

Quantitative joint histopathology

At 17 weeks, rats were euthanized, and knee joints were excised for histology. First, knee joints were dissected and fixed in 10% neutral buffered formalin for 48 h at room temperature. Following fixation, joints were placed in ethanol until all joints were ready for decalcification. For decalcification, joints were placed in 10% formic acid for 14 days, washed in phosphate buffered saline, and then vacuum infiltrated in paraffin wax. After embedding in paraffin, 10 μm frontal sections were collected. Sections representing the loading region were then stained with safranin-O and a fast green counterstain. For synovitis grading, neighboring slides underwent hematoxylin and eosin staining. Joint remodeling associated with surgical induction of post-traumatic OA was evaluated using open-source software developed by our lab.[29,30] Briefly, this software uses morphometric analysis of bone and cartilage along with spatial evaluation of joint-level changes through location dependent measures. For location dependent measures, bone and cartilage thickness measurements were obtained at each 5% interval from the interior aspect to the margins of the tibia. With cartilage, this thickness was measured between cartilage surface and the osteochondral interface. Regarding bone, bone thickness was calculated by subtracting the marrow thickness from the subchondral bone thickness at each 5% interval. For synovitis, the synovial lining of the medial joint capsule was imaged at 20x and scored using Krenn guidelines.[31]

Statistical analysis

Being unable to *apriori* estimate the sex-related interactions in brain remodeling for the MCLT+MMT model, our experiment was designed to perform separate analyses for male and female rats. Our statistical model varied based upon whether the dependent variable was longitudinal and how many multiple comparisons needed correcting, as described hereafter. All statistical analyses were performed using RStudio (v. 4.0.2). To adjust for inter-animal variability at baseline, tactile sensitivity and MRI data were centered by subtracting baseline values from each longitudinal timepoint for each animal. Tactile sensitivity and MRI data were then analyzed using a linear mixed effects model, where animal ID was treated as a random factor and surgery and time were treated as fixed factors. For tactile sensitivity, the significance of surgery and time along with their interaction was analyzed using type III analysis of variance via Satterthwaite's method ($p < 0.05$ considered significant). If the interaction was significant, post-hoc comparisons were performed via Tukey's HSD corrected comparisons of least squared means. For the MRI data, post-hoc analysis was performed for each volume, BOLD signal region, and functional connectivity to evaluate group differences between MCLT+MMT and skin-incision groups at 6- and 14-weeks post-surgery, respectively. To minimize type II error, MRI regions evaluated were restricted to those relevant to pain processing. Additionally, a Benjamini-Hochberg correction was used to control the false discovery rate (FDR) for each MRI data type (volumetric, BOLD, functional connectivity), separately. Regions reported as statistically significant had a corrected p-value (following FDR correction) less than 0.05. Separate FDR corrections were performed for regions associated with the emotional/affective aspect of pain and sensory-discriminate regions as visualized in Figure 2.

Morphometric histological data were analyzed using linear models

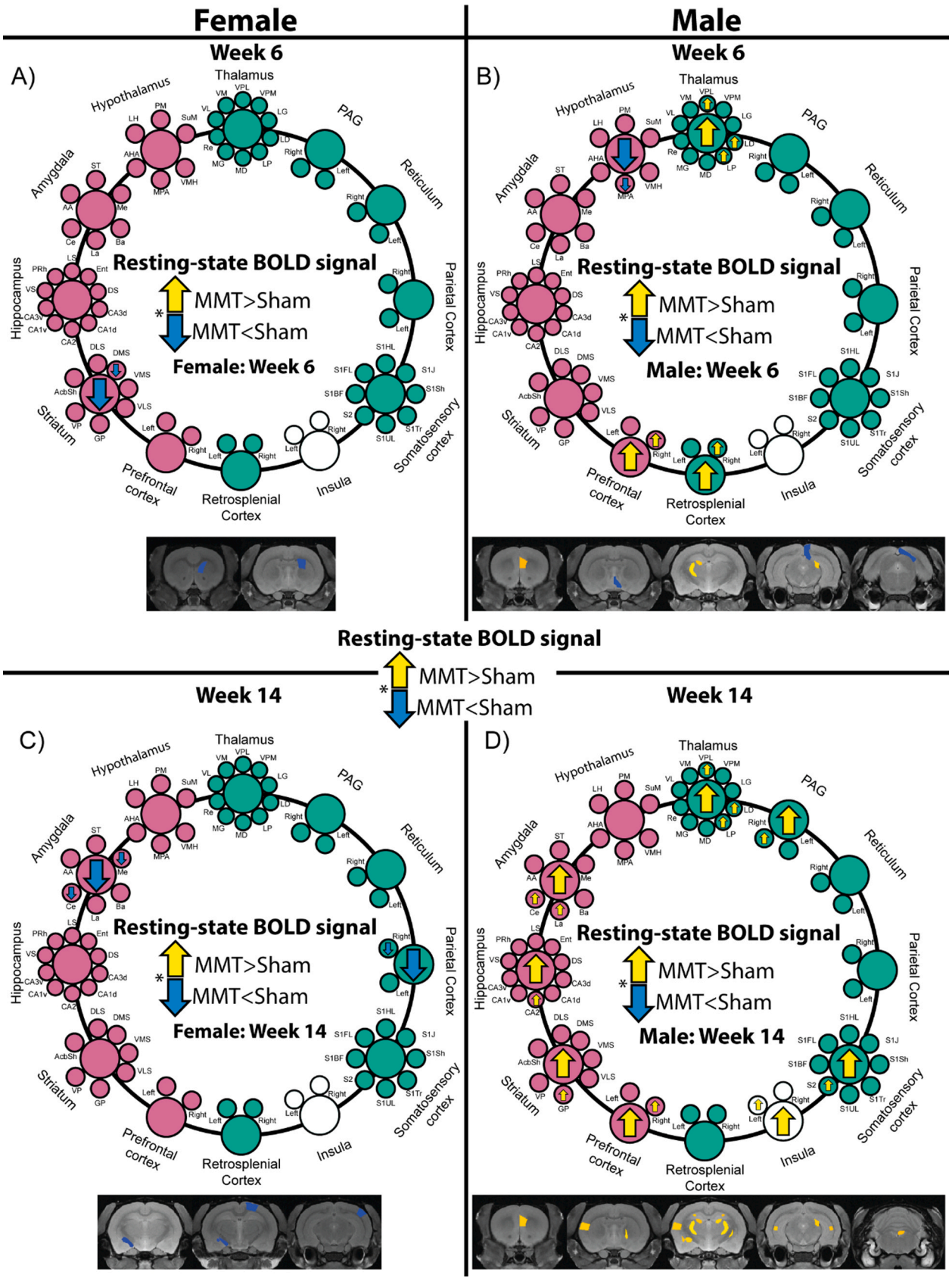

Fig. 6. Group differences in BOLD signal are shown for females at week 6 **(A)** and week 14 **(C)** and males at week 6 **(B)** and week 14 **(D)**. Higher BOLD signals in the MCLT+MMT group relative to skin-incision sham are indicated using a yellow arrow and lower BOLD signals are shown with a blue arrow. Regions in magenta are related to the emotional/affective aspects of pain, whereas green is associated with sensory discrimination. Statistical significance was determined following the Benjamini-Hochberg correction ($p_{adj} < 0.05$).

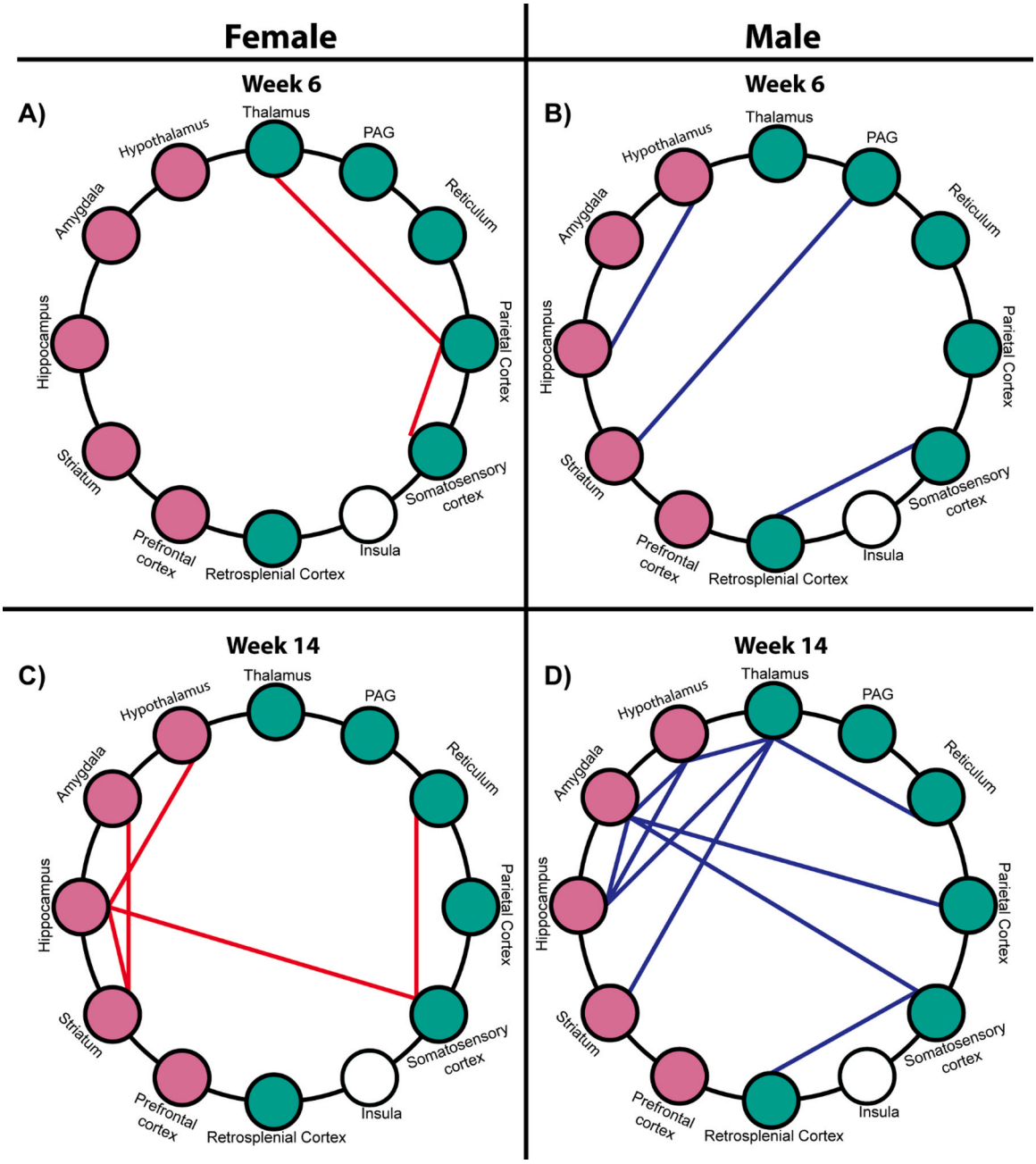

Fig. 7. Group differences in functional connectivity are shown for females at week 6 **(A)** and week 14 **(C)** and males at week 6 **(B)** and week 14 **(D)**. Higher functional connectivities in the MCLT+MMT group relative to skin-incision sham is indicated using a yellow arrow and lower connectivities are shown with a blue arrow. Regions in magenta are related to the emotional/affective aspects of pain, whereas green is associated with sensory discrimination. Statistical significance was determined following the Benjamini-Hochberg correction ($p_{adj} < 0.05$).

with surgery as a factor. A post-hoc Tukey's HSD was performed to evaluate differences between MCLT+MMT and skin-incision animals for male and female animals, separately. Group differences in location dependent joint changes were evaluated using 95% confidence intervals. For synovitis, grades were analyzed using a Kruskal-Wallis test, followed by Wilcoxon signed rank test.

Finally, please note that, due the significant dropout in males, our statistical power for male comparisons falls below our apriori calculated threshold of n=10 per group. For transparency and to help guide future work, we present our data collected on males, while also acknowledging the underpowered nature and a higher than intended Type II error rate in the male cohort.

Results

MCLT+MMT is associated with location dependent joint remodeling in cartilage and bone

Histological changes due to MCLT+MMT were visualized through evaluation of subchondral bone and cartilage area, thickness measurements of cartilage and subchondral bone from the interior aspect of the medial compartment to the medial margin. No changes to cartilage thickness were observed in the lateral compartment. For MCLT+MMT females, medial tibial cartilage area decreased and subchondral bone area increased compared to skin-incision shams (p=0.004, cartilage; p=0.03, bone) (Figure 3A, **C**). For males, medial tibial cartilage area and

Table 2
Statistically significant group differences in BOLD signal, including effect size and p-values before and after false discovery rate correction.

	Mean (95% confidence interval)				
	MCLT+MMT	Skin-incision	η^2	p_{raw}	p_{adj}
BOLD comparison at week 6 (male)					
Ventroposterior lateral nucleus of thalamus (left)	0.032 [0.017, 0.047]	-0.021 [-0.032, −0.010]	0.42	$7.47*10^{-7}$	$4.01*10^{-5}$
Laterodorsal nucleus of thalamus (left)	0.030 [0.017, 0.043]	-0.006 [-0.016, 0.003]	0.32	$2.6*10^{-5}$	0.0014
Lateroposterior nucleus of thalamus (right)	0.017 [0.004, 0.030]	-0.025 [0.014, 0.037]	0.32	$3*10^{-5}$	0.0016
Retrosplenial cortex caudal (right)	-0.025 [-0.037, −0.012]	0.004 [-0.004, 0.013]	0.25	0.0003	0.0164
Medial preoptic area (right)	-0.018 [-0.029, −0.007]	0.008 [0.0002, 0.016]	0.24	0.00036	0.0216
Prelimbic cortex (right)	0.013 [0.002, 0.025]	-0.013 [-0.021, −0.005]	0.24	0.00047	0.0281
BOLD comparison at week 14 (male)					
Ventroposterior lateral nucleus of thalamus (left)	0.044 [0.030, 0.057]	-0.010 [-0.022, 0.002]	0.43	$5.4*10^{-7}$	$2.9*10^{-5}$
Ventroposterior lateral nucleus of thalamus (right)	0.035 [0.018, 0.053]	-0.025 [-0.041, −0.009]	0.37	$5.4*10^{-6}$	0.00029
Laterodorsal nucleus of thalamus (left)	0.024 [0.012, 0.035]	-0.009 [-0.020 0.001	0.28	0.00011	0.00588
Laterodorsal nucleus of thalamus (right)	0.035 [0.022, 0.048]	-0.011 [-0.023, 0.001]	0.37	$4.3*10^{-6}$	0.00023
Lateroposterior nucleus of thalamus (right)	0.025 [0.014, 0.037]	-0.015 [-0.026, −0.005]	0.36	$6.1*10^{-6}$	0.00105
Prelimbic cortex (right)	0.024 [0.014, 0.034]	-0.013 [-0.021, −0.005]	0.33	$1.9*10^{-5}$	0.00117
CA2 of hippocampus (left)	0.017 [0.0001, 0.033]	-0.023 [-0.038, −0.008]	0.22	0.00084	0.0455
CA2 of hippocampus (right)	0.012 [0.002, 0.023]	-0.020 [-0.029, −0.010]	0.31	$3.4*10^{-5}$	0.00207
Lateral nucleus of amygdala (left)	0.007 [-0.006, 0.020]	-0.028 [-0.040, −0.016]	0.25	0.00027	0.005
Central nucleus of amygdala (left)	0.025 [0.009, 0.041]	-0.018 [-0.032, −0.003]	0.25	0.00029	0.0065
Globus pallidus (right)	0.028 [0.010, 0.046]	-0.019 [-0.035, −0.002]	0.24	0.00036	0.014
Secondary somatosensory cortex (left)	0.015 [-0.0004, 0.031]	-0.023 [-0.037, −0.009]	0.22	0.00066	0.036
Central gray (right)	0.011 [-0.001, 0.024]	-0.019 [-0.030, −0.007]	0.22	0.00086	0.046
BOLD comparison at week 6 (female)					
Dorsomedial striatum (right)	-0.029 [-0.040, −0.018]	0.003 [-0.011, 0.017]	0.16	0.0008	0.048
BOLD comparison at week 14 (female)					
Medial nucleus of amygdala (left)	-0.009 [-0.019, 0.002]	0.024 [0.012, 0.037]	0.21	0.00013	0.008
Central nucleus of amygdala (left)	-0.023 [-0.034, −0.013]	0.009 [-0.004, 0.022]	0.19	0.00027	0.016
Parietal cortex (right)	-0.019 [-0.029, −0.010]	0.007 [-0.005, 0.018]	0.16	0.0008	0.043

subchondral bone area were not significantly different (p=0.78, cartilage; p=0.31, bone) (Figure 3B, **D**).

Synovitis scores for the synovial lining of the medial joint capsule revealed low-grade synovitis in all MCLT+MMT rats except 2 (1 male and 1 female) (Figures 3E and 3F). For females, a significant difference was observed between the MCLT+MMT group and skin-incision sham. Female rats in the MCLT+MMT group (Q1-Q3 = 2–4) had greater synovitis scores than the female skin-incision sham group (Q1-Q3 = 1, $p < 0.001$). No significant differences were observed between the male MCLT+MMT group and the male skin-incision shams, though male MCLT+MMT rats (Q1–Q3 = 2–3) did tend to have greater synovitis scores than skin-incision sham (Q1–Q3 = 1, p = 0.16); this lack of significance may related to the underpowered nature of the male cohort.

Regarding location-dependent changes, lesion morphometry plots can be used to visualize thickness measurements for bone and cartilage in 5% intervals from the interior aspect of the medial compartment (0%) to the medial margin (100%) of the tibia, with shaded regions representing 95% confidence intervals (Fig. 4). For cartilage thickness in the medial tibial cartilage, both female and male MCLT+MMT groups showed regions of decreased cartilage – represented by non-overlapping 95% confidence interval bands (Fig. 4 **A&B**). Conversely, subchondral bone thickness increased in specific regions of the medial compartment for the MCLT+MMT groups in both females (Fig. 4C) and males (Fig. 4D**).**

MCLT+MMT did not alter tactile sensitivity compared to skin-incision sham group

While histology was used to evaluate pathological features of OA, tactile sensitivity was analyzed to evaluate behavioral changes. Here, tactile sensitivity data is shown as the 50% withdrawal threshold throughout OA progression in Supplemental Figure 1A and 1B. The 50% withdrawal thresholds did not statistically differ between surgical groups at any given timepoint; however, time had a significant effect. For females, the 50% withdrawal threshold for both groups decreased from baseline to 4 weeks (p=0.003), 8 weeks (p=0.001), 12 weeks (p=0.0007), and 16 weeks (p=0.00002). Whereas for males, the 50% withdrawal threshold decreased for both groups from baseline to week 4 (p=0.03) and week 8 (p=0.04). These decreases in the 50% withdrawal threshold compared to baseline are suggestive of increased sensitivity after surgery, but not related to the type of surgery performed.

Brain structure in pain-processing regions differs between MCLT+MMT and skin-incision sham

Group differences in gray matter volume were observed in both sensory-discriminative and emotional-affective regions of the brain at 6- and 14-weeks post-surgery. Regions experiencing volumetric changes are visualized using Fig. 5A-D. In males at 6-weeks post-surgery, region volume was higher in the MCLT+MMT compared to skin-incision controls for the right secondary somatosensory cortex and right ventral CA1

Table 3
Functional connectivity (FC) differences after false discovery rate correction.

	Mean [95% confidence interval]				
	MCLT+MMT	Skin-incision	η^2	p_{raw}	p_{adj}
FC comparison at week 6 (male)					
Ventral subiculum (left) and nucleus accumbens (left)	0.234 [0.139, 0.328]	-0.057 [-0.124, 0.011]	0.37	$6.9*10^{-6}$	0.018
Entorhinal cortex (left) and lateral hypothalamus (left)	-0.098 [-0.186, −0.011]	0.163 [0.10, 0.225]	0.35	$1.2*10^{-5}$	0.031
FC comparison at week 14 (male)					
Entorhinal cortex (left) and lateral hypothalamus (left)	-0.189 [-0.267, −0.111]	0.203 [0.129, 0.278]	0.55	$2.5*10^{-9}$	$6.74*10^{-6}$
Anterior amygdala (left) and lateral hypothalamus (right)	-0.151 [-0.235, −0.067]	0.229 [0.149, 0.308]	0.5	$2.7*10^{-8}$	$7.31*10^{-5}$
Perirhinal cortex (left) and anterior hypothalamic area (left)	-0.119 [-0.210, −0.028]	0.272 [0.186, 0.359]	0.48	$9.7*10^{-8}$	0.00026
Ventral CA3 of hippocampus (left) and ventral posteriolateral thalamus (left)	-0.004 [-0.078, 0.071]	0.297 [0.226, 0.369]	0.44	$3.4*10^{-7}$	0.00092
Ventral posteriolateral thalamus (left) and ventromedial hypothalamus (right)	-0.099 [-0.210, 0.011]	0.327 [0.222, 0.431]	0.42	$8.1*10^{-7}$	0.00218
Ventral posteriolateral thalamus (left) and anterior hypothalamic area (right)	-0.091 [-0.216, 0.036]	0.390 [0.271, 0.510]	0.42	$9.9*10^{-7}$	0.00266
Medial nucleus of amygdala (right) and ventral CA1 of hippocampus (right)	-0.156 [-0.304, −0.009]	0.397 [0.256, 0.538]	0.41	$1.5*10^{-6}$	0.004
Ventral CA3 of hippocampus (left) and anterior hypothalamic area (left)	-0.106 [-0.210, −0.002]	0.279 [0.180, 0.378]	0.4	$1.9*10^{-6}$	0.005
Midbrain reticular formation (right) and medial geniculate (right)	-0.123 [-0.241, −0.005]	0.307 [0.194, 0.419]	0.4	$2.4*10^{-6}$	0.0065
Ventrolateral thalamus (left) and ventromedial hypothalamus (right)	-0.0823 [-0.203, 0.039]	0.349 [0.233, 0.464]	0.38	$3.7*10^{-6}$	0.0099
Ventromedial hypothalamus (left) and somatosensory cortex upper lip (right)	-0.176 [-0.278, −0.074]	0.181 [0.084, 0.279]	0.38	$4.9*10^{-6}$	0.0133
Perirhinal cortex (left) and reuniens nucleus thalamus (right)	-0.030 [-0.128, 0.067]	0.306 [0.214, 0.399]	0.37	$5.9*10^{-6}$	0.016
Somatosensory cortex hindlimb (left) and premammillary nucleus hypothalamus (left)	-0.188 [-0.292, −0.085]	0.166 [0.068, 0.264]	0.37	$7*10^{-6}$	0.018
Medial preoptic area (right) and mediodorsal thalamus (right)	-0.116 [-0.246, 0.0136]	0.326 [0.203 0.448]	0.36	$7.5*10^{-6}$	0.0202
Parietal cortex (left) and lateral nucleus amygdala (right)	-0.268 [-0.428, −0.108]	0.278 [0.125, 0.430]	0.36	$7.8*10^{-6}$	0.0209
Somatosensory cortex trunk (left) and lateral nucleus amygdala (right)	-0.252 [-0.420, −0.084]	0.321 [0.161, 0.481]	0.36	$7.9*10^{-6}$	0.0212
Insula (left) and perirhinal cortex (right)	-0.124 [-0.221, −0.027]	0.205 [0.113, 0.297]	0.36	$8.5*10^{-6}$	0.0229
Ventral posteriomedial thalamus (left) and ventromedial hypothalamus (right)	-0.099 [-0.210, 0.013]	0.278 [0.172, 0.384]	0.36	$8.8*10^{-6}$	0.0237
Ventral pallidum (left) and anterior nucleus thalamus (right)	-0.043 [-0.141, 0.055]	0.285 [0.192, 0.379]	0.36	$1*10^{-5}$	0.0277
Entorhinal cortex (left) and ventromedial nucleus of hypothalamus (left)	-0.118 [-0.198, −0.037]	0.151 [0.075, 0.227]	0.36	$1*10^{-5}$	0.0282
Ventral posteriolateral thalamus (left) and premammillary nucleus hypothalamus (right)	-0.104 [-0.205, −0.003]	0.233 [0.137, 0.329]	0.35	$1.1*10^{-5}$	0.0298
Ventral posteriolateral thalamus (left) and supramammillary nucleus hypothalamus (right)	-0.082 [-0.173, 0.008]	0.217 [0.132, 0.303]	0.35	$1.2*10^{-5}$	0.032
Medial nucleus amygdala (right) and ventral subiculum (right)	-0.171 [-0.301, −0.040]	0.263 [0.138, 0.389]	0.35	$1.3*10^{-5}$	0.0339
Ventral pallidum (left) and anterior nucleus thalamus (left)	-0.034 [-0.111, 0.044]	0.223 [0.149, 0.296]	0.35	$1.3*10^{-5}$	0.0356
Somatosensory cortex hindlimb (left) and retrosplenial cortex caudal (right)	-0.120 [-0.241, 0.002]	0.279 [0.164, 0.394]	0.35	$1.4*10^{-5}$	0.0379
Ventrolateral nucleus thalamus (left) and premammillary nucleus hypothalamus (right)	-0.063 [-0.173, 0.046]	0.295 [0.192, 0.399]	0.35	$1.4*10^{-5}$	0.0385
Perirhinal cortex (left) and medial preoptic area (left)	-0.115 [-0.213, −0.016]	0.209 [0.115, 0.303]	0.35	$1.5*10^{-5}$	0.0398
Secondary somatosensory cortex (left) and anterior hypothalamic area (left)	-0.092 [-0.198, 0.014]	0.255 [0.155, 0.356]	0.35	$1.5*10^{-5}$	0.0405
Somatosensory cortex hindlimb (left) and supramammillary nucleus hypothalamus (left)	-0.204 [-0.298, −0.110]	0.105 [0.015, 0.194]	0.34	$1.5*10^{-5}$	0.041
Ventrolateral thalamus (left) and anterior hypothalamic area (right)	-0.096 [-0.225, 0.033]	0.324 [0.202, 0.446]	0.34	$1.6*10^{-5}$	0.043
Medial nucleus of amygdala (right) and ventral CA3 hippocampus (right)	-0.133 [-0.289, 0.023]	0.374 [0.225, 0.523]	0.34	$1.7*10^{-5}$	0.047
Ventral CA1 hippocampus (left) and anterior hypothalamic area (left)	-0.076 [-0.188, 0.036]	0.284 [0.179, 0.390]	0.34	$1.9*10^{-5}$	0.0499
FC comparison at week 6 (female)					
Parietal cortex (right) and somatosensory cortex trunk (right)	0.206 [0.106, 0.306]	-0.164 [-0.284, −0.044]	0.26	$1.4*10^{-5}$	0.0368

(*continued on next page*)

Table 3 (*continued*)

	Mean [95% confidence interval]				
	MCLT+MMT	Skin-incision	η^2	p_{raw}	p_{adj}
FC comparison at week 14 (female)					
Entorhinal cortex (right) and supramammillary nucleus hypothalamus (right)	0.268 [0.191 0.345]	-0.024 [-0.114, 0.065]	0.27	$5.8*10^{-6}$	0.0156
Dorsal subiculum (left) and somatosensory cortex shoulder (right)	0.083 [0.002, 0.163]	-0.213 [-0.306, −.120]	0.26	$1*10^{-5}$	0.028
Midbrain reticular formation (left) and somatosensory cortex barrel field (right)	0.059 [-0.020 0.137]	-0.229 [-0.320, −0.138]	0.26	$1.1*10^{-5}$	0.0287

of the hippocampus. At week 14, additional group differences were observed for males in regions involved in pain modulation, sensory perception, reward and motivation, and the emotional aspects of pain. Gray matter volume was higher for MCLT+MMT males in the right hemisphere of the central gray, left somatosensory cortex trunk, and right CA2 of the hippocampus along with lower volume in the ventromedial striatum. In females, MCLT+MMT animals at week 6 had higher gray-matter volume compared to skin-incision for the right ventral posteriomedial nucleus of the thalamus, which is a relay station for somatosensory information. Conversely, gray matter volume was lower in MCLT+MMT females compared to skin-incision in the right medial geniculate, a relay station for auditory information. At week 14 additional group differences were seen with MCLT+MMT females having higher gray matter volumes in the left somatosensory cortex upper lip and lower volume in the right medial nucleus of the amygdala. Statistically significant group differences in gray matter volume, with corresponding p-values and effect sizes, are described in Table 1 ($p_{adj}<0.05$).

BOLD signal and functional connectivity are altered in MCLT+MMT compared to skin-incision

Comparison of BOLD signal between MCLT+MMT and skin-incision controls at week 6 and week 14, respectively, were significantly different in a variety of regions (Fig. 6A-D). For males at 6 weeks post-surgery, group differences between MCLT+MMT and skin-incision controls were observed in the thalamus, cortex, and medial preoptic area of the hypothalamus. Specifically, BOLD signal in males was higher in MCLT+MMT compared to skin-incision controls for multiple thalamic nuclei involved in the sensory-discriminate component of pain including the left hemisphere of both the ventroposterior lateral and laterodorsal nuclei and the right hemisphere of the lateroposterior nucleus. Cortically, BOLD signal in males was lower for MCLT+MMT compared to skin-incision, in the right hemisphere of the retrosplenial cortex and higher in the right prelimbic cortex. As OA further progressed, at week 14, BOLD signal group differences for males were observed in regions related to sensory discrimination, pain modulation, and the limbic system. Within the thalamus, both hemispheres of the ventroposterior lateral and laterodorsal nuclei and the right lateroposterior nucleus were higher in MCLT+MMT males compared to skin-incision controls. Cortically, BOLD signal in the prelimbic cortex remained higher in the MCLT+MMT group. Compared to week 6, more regions within the limbic system had significant group differences with BOLD signal being higher for MCLT+MMT animals in both hemispheres of the CA2 of the hippocampus, left lateral nucleus of the amygdala, left central nucleus of the amygdala, and right globus pallidus. Finally, the left hemisphere of both the central gray, involved in pain modulation, and the secondary somatosensory cortex, related to sensory discrimination, were higher in MCLT+MMT animals compared to skin-incision. For females, BOLD signal was decreased in the right dorsomedial striatum in MCLT+MMT animals compared to skin-incision at week 6. At week 14, limbic system regions with group differences were the left hemispheres of the medial and central amygdala nuclei, both with lower BOLD signal in the MCLT+MMT group. Additionally, the parietal cortex, which is related to sensory-discriminate processing, was also lower in MCLT+MMT females compared to their skin-incision controls.

Regarding functional connectivity, a variety of connections were different in MCLT+MMT animals compared to skin-incision at week 6 and week 14, respectively (Fig. 7A-D). In males at week 6, group differences are observed within the mesocorticolimbic system, a major dopaminergic pathway. Specifically, higher connectivity was observed in MCLT+MMT males compared to skin-incision controls for the connection between the left hemispheres of the ventral subiculum and the nucleus accumbens. Additionally, lower connectivity was observed between the left hemispheres of the entorhinal cortex and lateral hypothalamus. At week 14, additional group differences were seen involving the mesocorticolimbic system. Briefly, lower functional connectivity in males was observed for MCLT+MMT compared to skin-incision controls in connections involving regions of the mesocorticolimbic circuit including the entorhinal cortex, lateral hypothalamus, anterior amygdala, perirhinal cortex, anterior hypothalamic area, medial nucleus of the amygdala, CA1 of the hippocampus, and CA3 of the hippocampus. Additionally, lower functional connectivity in males was seen in MCLT+MMT compared to skin-incision for connections between the thalamus and regions within the mesocorticolimbic system regions such as the ventromedial hypothalamus, CA3 of the hippocampus, anterior hypothalamic area, perirhinal cortex, medial preoptic area, ventral pallidum, and the premammillary nucleus of the hypothalamus. For females at week 6, functional connectivity was higher between the right parietal cortex and right somatosensory cortex trunk for the MCLT+MMT group compared to skin-incision sham. As OA progressed to week 14, higher connectivity for females was also observed in MCLT+MMT compared to skin-incision for connections between the right entorhinal cortex and supramammillary nucleus, left dorsal subiculum and right somatosensory cortex shoulder, and the left midbrain reticular formation and right somatosensory cortex barrel field.

All statistically significant group differences in BOLD signal are reported in Table 2 ($p_{adj} < 0.05$). Specific connections with statistically significant FC group differences are shown in Table 3 and include corresponding p-values and effect sizes ($p_{adj} < 0.05$).

Discussion

Multiple studies have described brain remodeling in rat models of OA. However, no study has evaluated brain remodeling in aged rats in a surgical OA model. Here, we provide a preliminary evaluation of brain changes in aged male and female animals, along with assessment of joint remodeling and tactile sensitivity. While tactile sensitivity data did not significantly differ between surgical groups, widespread joint remodeling and group differences in brain structure and function was observed in MCLT+MMT animals compared to skin-incision controls. These neuroimaging results include previously unreported regions relevant to pain transmission and modulation, the emotional and affective aspects of pain, and reward and motivation.

This study further supports evidence of structural and functional brain remodeling in OA. Although mechanisms driving the remodeling are still unknown, changes in previously identified regions and new regions were both observed. In comparison to Da Silva et al.,[8] we did observe fewer changes in periaqueductal gray connectivity; however,

this difference could be due to the use of a different model. While we used the MCLT+MMT model, Da Silva et al.[8] used the MIA model. MIA injection result in a local inhibition of glycolysis, causing cell stress and death. These events lead to local inflammatory events that may differ from the inflammation seen in surgical models of OA, which are driven by biomechanical imbalance and joint instability. Others have proposed this difference as a driving factor in the lack of transcriptional overlap between MIA affected joints and human OA cartilage samples.[32] These differences may also differentially alter central and peripheral pathways between chemical and surgical models of knee OA. Still, the clinical features of OA are highly heterogeneous, and the different models of OA may be illuminating different drivers of pain transmission and modulation in the brain. A key feature that varies from the past work in the MIA model appears to center on PAG connectivity, with marked differences between our data in MCLT+MMT model and prior reports in the MIA model.

Our results align with the theory that chronic OA results in brain changes beyond regions related to pain transmission and modulation. The longitudinal nature of our experimental design demonstrates that disease progression related group differences are time-dependent. Our previous work showed early-stage OA-related symptoms and joint remodeling were detectable around 6 weeks post-surgery.[19] Upadhyay et al.[11] reported functional brain remodeling at 4 weeks post-surgery, in the same surgical OA model but using young rats, suggesting that brain changes may precede changes in animal behavior and joint-level damage related to OA progression. Although we are unable to definitively conclude key features indicative of pain chronification in this preclinical model of OA, differences in structural and functional remodeling at weeks 6 and 14 exist. At week 6, our results show structural and functional changes are primarily in regions related to pain transmission and modulation, including functional changes in the thalamus and PAG that are similar to those reported by Upadhyay et al and Da Silva et al.[8,11] Whereas, at week 14, there is an increase in the number of remodeled regions related to both pain transmission and modulation along with the emotional and affective aspects of pain. The widespread functional group differences in mesocorticolimbic system regions – including the striatum, hippocampus, prefrontal cortex, and amygdala – aligns with previous literature focused on neuropathic pain models, like the chronic constriction and spare nerve injury models.[33–35] Overall, these findings suggest that pain at 6 weeks post-surgery in the MCLT+MMT model may be driven by acute components, whereas pain at 14 weeks post-surgery may be related to a complex integration of pain processing across sensory discriminate and emotional and affect regions of the brain. This aligns with prior reports in OA patients and low back pain patients.[16–18]

Despite our brain imaging data, our behavioral results were inconclusive. There are a number of potential factors that may explain the lack of a group difference in tactile sensitivity. First, age-related effects on pain sensitivity in preclinical models has previously been discussed[36–39] and may have affected the tactile sensitivity measures in this study. Additionally, previous literature has shown an effect of skin-incision on mechanical sensitivity.[40] Since this study used a skin-incision sham instead of a naïve control, incision-related pain, combined with age-related sensitization, could partially explain the decrease in 50% withdrawal threshold in both surgical conditions. Another potential confounding factor was the use of Fischer rats. Compared to other rat strains, Fischer rats have a high incidence rate of neoplasms when aged beyond 18 months. Animals with undiscovered, early-stage neoplasms may exhibit increased sensitization, thereby skewing tactile sensitivity measures across all groups. Beyond age, experimental design, and strain considerations, previous literature suggests that tactile sensitivity is a measure of reflex instead of pain sensitivity.[36] As such tactile sensitivity may be controlled at the spinal cord level and not the brain. If true, this may support our results, showing remodeling in pain-processing related regions without corresponding behavioral results.

Although sex effects were not directly evaluated, results from this study encourage future investigations into sex-related differences regarding structural and functional brain changes in the MCLT+MMT model. Our study was designed to include equal number of male and female animals, but due to dropout, the male cohort was smaller, meaning our detectable effect size was smaller for females that males. Beyond sample size, the direction of brain remodeling also differs with sex. For example, in males, BOLD signal increased in MCLT+MMT compared to skin-incision and decreased in females for subregions of the thalamus, somatosensory cortex, parietal cortex, hippocampus, and amygdala. Furthermore, functional connectivity was higher in MCLT+MMT animals compared to skin-incision animals in females, but lower in males. Although the mechanism behind this difference is unknown, there appears to be sexual dimorphism related to chronic pain processing in the brain. Finally, in addition to limitations introduced by male dropout rates, other limitations of our study should be noted. First, while OA pain is known to be heterogeneous, it is not yet clear whether there is a shift in the connectivity of the brain as OA transitions from acute to chronic in the MCLT+MMT model, or if this shift is influenced by the age of the animal or nociceptive and neuropathic mechanisms of pain occurring in the periphery. Ongoing work through projects like NIH's ReJOIN Consortium are beginning to assess these features in multiple models of knee OA.

In conclusion, our work is the first to examine brain remodeling in the MCLT+MMT model of OA using aged animals. At 6 and 14 weeks, we observed altered region volumes, BOLD signal, and functional connectivity for the MCLT+MMT animals compared to skin-incision controls. Additionally, location dependent decreases in cartilage thickness and increases in subchondral bone area occurred in MCLT+MMT animals – which aligns with what we expect from this model. While our results show remodeling of both the joint and brain, how these changes relate to pain-related symptoms is still largely unknown. In the case of follow-up studies utilizing aged animals to evaluate chronic disease progression in OA, we encourage consideration of how the strain and age of the animal may impact central and peripheral sensitization and dropout due to conditions such as leukemia. Ultimately, our results demonstrate evidence of brain remodeling in preclinical models of OA and encourage follow-up studies that can better characterize the underlying mechanisms driving these changes.

Author contributions

JLG, PVH, TDY, MF, YCA, and KDA contributed to the study design. JLG and PVH collected and analyzed the MRI data with assistance from SHP. TDY performed surgeries. JLG and TDY performed tissue dissections. JLG collected, processed, and analyzed the behavioral data. Behavioral and histological data were interpreted by JLG, TDY, SHP, and KDA. MRI data was interpreted by JLG, PVH, MF, YCA, SHP, and KDA. The manuscript was prepared by JLG with critical feedback from PVH, TDY, MF, YCA, SHP and KDA. All authors agree with the content and interpretation of the data as presented.

Funding

The National Institute of Arthritis and Musculoskeletal and Skin Diseases of the National Institutes of Health (NIAMS/NIH) supported this study under award numbers R01AR071431, and UC2AR082196. An administrative supplement from the National Institute on Aging supported brain imaging in a NIAMS funded study through award number R01AR071431–04S2. Additionally, this work was supported by an NSF Graduate Research Fellowship (DGE-1842473) and a graduate student fellowship from the Herbert Wertheim College of Engineering and J. Crayton Pruitt Family Department of Biomedical Engineering at the University of Florida. This work was performed in the McKnight Brain Institute at the National High Magnetic Field Laboratory's AMRIS Facility, which is supported by National Science Foundation Cooperative Agreement No. DMR-1644779 and the State of Florida.

Acknowledgments

The authors thank Dr. Huadong Zeng for training and support with magnetic resonance imaging; Dr. Kiara Chan, Taylor Harrell, Dr. Carlos Cruz, and Dr. Folly Patterson for assistance during surgeries; and Dr. Folly Patterson and Dr. Janak Gaire for assistance with synovitis grading.

Conflicts of Interest Statement

The authors have no conflicts of interest to declare.

Appendix A. Supporting information

Supplementary data associated with this article can be found in the online version at doi:10.1016/j.jpain.2025.105594.

Availability of data and materials

The data that support the findings of this study are available from the corresponding author, KDA, upon reasonable request.

References

1. Yeater TD, Cruz CJ, Cruz-Almeida Y, Allen KD. Autonomic nervous system dysregulation and osteoarthritis pain: mechanisms, measurement, and future outlook. *Curr Rheuma Rep*. 2022;24(6):175–183. https://doi.org/10.1007/s11926-022-01071-9.
2. Yeater TD, Zubcevic J, Allen KD. Measures of cardiovascular function suggest autonomic nervous system dysregulation after surgical induction of joint injury in the male Lewis rat. *Osteoarthr Cartil*. 2022;30(4):586–595. https://doi.org/10.1016/j.joca.2021.12.008.
3. Yeater TD, Griffith JL, Cruz CJ, Patterson FM, Aldrich JL, Allen KD. Hypertension contributes to exacerbated osteoarthritis pathophysiology in rats in a sex-dependent manner. *Arthritis Res Ther*. 2023;25(1):7. https://doi.org/10.1186/s13075-022-02966-9.
4. Cruz CJ, Dewberry LS, Otto KJ, Allen KD. Neuromodulation as a potential disease-modifying therapy for osteoarthritis. *Curr Rheuma Rep*. 2023;25(1):1–11. https://doi.org/10.1007/s11926-022-01094-2.
5. Barroso J, Vigotsky AD, Branco P, et al. Brain gray matter abnormalities in osteoarthritis pain: a cross-sectional evaluation. *Pain*. 2020;161(9):2167–2178. https://doi.org/10.1097/j.pain.0000000000001904.
6. Barroso J, Wakaizumi K, Reis AM, et al. Reorganization of functional brain network architecture in chronic osteoarthritis pain. *Hum Brain Mapp*. 2021;42(4):1206–1222. https://doi.org/10.1002/hbm.25287.
7. Chatterjee I, Baumgartner L, Cho M. Detection of brain regions responsible for chronic pain in osteoarthritis: an fMRI-based neuroimaging study using deep learning. *Front Neurol*. 2023;14, 1195923. https://doi.org/10.3389/fneur.2023.1195923.
8. DaSilva JT, Tricou C, Zhang Y, Tofighbakhsh A, Seminowicz DA, Ro JY. Pain modulatory network is influenced by sex and age in a healthy state and during osteoarthritis progression in rats. (in eng). *Aging Cell*. Feb 2021;20(2), e13292. https://doi.org/10.1111/acel.13292.
9. Hall M, Dobson F, Klyne DM, Zheng CJ, Lima YL, Egorova-Brumley N. Neurobiology of osteoarthritis: a systematic review and activation likelihood estimation meta-analysis. *Sci Rep*. 2023;13(1), 12442. https://doi.org/10.1038/s41598-023-39245-9.
10. Pujol J, Martinez-Vilavella G, Llorente-Onaindia J, et al. Brain imaging of pain sensitization in patients with knee osteoarthritis. *Pain*. 2017;158(9):1831–1838. https://doi.org/10.1097/j.pain.0000000000000985.
11. Upadhyay J, Baker SJ, Rajagovindan R, et al. Pharmacological modulation of brain activity in a preclinical model of osteoarthritis. *Neuroimage*. 2012;64:341–355. https://doi.org/10.1016/j.neuroimage.2012.08.084.
12. McDougall JJ. Osteoarthritis is a neurological disease - an hypothesis. *Osteoarthr Cartil Open*. 2019;1(1-2), 100005. https://doi.org/10.1016/j.ocarto.2019.100005.
13. Thakur M, Dickenson AH, Baron R. Osteoarthritis pain: nociceptive or neuropathic? *Nat Rev Rheuma*. 2014;10(6):374–380. https://doi.org/10.1038/nrrheum.2014.47.
14. Baliki MN, Chang PC, Baria AT, Centeno MV, Apkarian AV. Resting-sate functional reorganization of the rat limbic system following neuropathic injury. *Sci Rep*. 2014;4:6186. https://doi.org/10.1038/srep06186.
15. Yeater TD, Clark DJ, Hoyos L, et al. Chronic pain is associated with reduced sympathetic nervous system reactivity during simple and complex walking tasks: potential cerebral mechanisms. *Chronic Stress*. 2021;5, 24705470211030273. https://doi.org/10.1177/24705470211030273.
16. Porreca F, Navratilova E. Reward, motivation, and emotion of pain and its relief. *Pain*. 2017;158(S1):S43–S49. https://doi.org/10.1097/j.pain.0000000000000798.
17. Baliki MN, Geha PY, Fields HL, Apkarian AV. Predicting value of pain and analgesia: nucleus accumbens response to noxious stimuli changes in the presence of chronic pain. *Neuron*. 2010;66(1):149–160. https://doi.org/10.1016/j.neuron.2010.03.002.
18. Baliki MN, Petre B, Torbey S, et al. Corticostriatal functional connectivity predicts transition to chronic back pain. *Nat Neurosci*. 2012;15(8):1117–1119. https://doi.org/10.1038/nn.3153.
19. Kloefkorn HE, Jacobs BY, Loye AM, Allen KD. Spatiotemporal gait compensations following medial collateral ligament and medial meniscus injury in the rat: correlating gait patterns to joint damage. *Arthritis Res Ther*. 2015;17:287. https://doi.org/10.1186/s13075-015-0791-2.
20. Chan KM, Yeater TD, Allen KD. Age alters gait compensations following meniscal injury in male rats. *J Orthop Res*. 2022;40(12):2780–2791. https://doi.org/10.1002/jor.25306.
21. Chaplan WR, Bach FW, Pogrel JW, Chung JM, Yaksh TL. Quantitative assessment of tactile allodynia in the rat paw. *J Neurosci Methods*. 1994;53(1):55–63.
22. Andersson JL, Skare S, Ashburner J. How to correct susceptibility distortions in spin-echo echo-planar images: application to diffusion tensor imaging. *Neuroimage*. 2003;20(2):870–888. https://doi.org/10.1016/S1053-8119(03)00336-7.
23. Smith SM, Jenkinson M, Woolrich MW, et al. Advances in functional and structural MR image analysis and implementation as FSL. *Neuroimage*. 2004;23(S1):S208–S219. https://doi.org/10.1016/j.neuroimage.2004.07.051.
24. Tustison NJ, Avants BB, Cook PA, et al. N4ITK: improved N3 bias correction. *IEEE Trans Med Imaging*. 2010;29(6):1310–1320. https://doi.org/10.1109/TMI.2010.2046908.
25. Kulkarni P, Kenkel W, Finklestein SP, et al. Use of anisotropy, 3D segmented atlas, and computational analysis to identify gray matter subcortical lesions common to concussive injury from different sites on the cortex. *PLoS One*. 2015;10(5), e0125748. https://doi.org/10.1371/journal.pone.0125748.
26. Pompilus M, Colon-Perez LM, Grudny MM, Febo M. Contextual experience modifies functional connectome indices of topological strength and efficiency. *Sci Rep*. 2020;10(1), 19843. https://doi.org/10.1038/s41598-020-76935-0.
27. Avants B, Tustison N, Song G, Yushkevich P, Song Z, Gee J. Advanced normalization tools: V1.0. *Insight J*. 2009;10.
28. Valdés-Hernández PA, Sumiyoshi A, Nonaka H, et al. An in vivo MRI template set for morphometry, tissue segmentation, and fMRI localization in rats. *Front Neuroinform*. 2011;5:26. https://doi.org/10.3389/fninf.2011.00026.
29. Kloefkorn HE, Allen KD. Quantitative histological grading methods to assess subchondral bone and synovium changes subsequent to medial meniscus transection in the rat. *Connect Tissue Res*. 2017;58(3-4):373–385. https://doi.org/10.1080/03008207.2016.1251425.
30. Kloefkorn HE, Jacobs BY, Xie DF, Allen KD. A graphic user interface for the evaluation of knee osteoarthritis (GEKO): an open-source tool for histological grading. *Osteoarthr Cartil*. 2019;27(1):114–117. https://doi.org/10.1016/j.joca.2018.09.005.
31. Krenn V, Morawietz L, Burmester G-R, et al. Synovitis score: discrimination between chronic low-grade and high-grade synovitis. *Histopathology*. 2006;49(4):358–364. https://doi.org/10.1111/j.1365-2559.2006.02508.x.
32. Barve RA, Minnerly JC, Weiss BA, et al. Transcriptional profiling and pathway analysis of monosodium iodoacetate-induced experimental osteoarthritis in rats: relevance to human disease. *Osteoarthr Cartil*. 2007;15(10):1190–1198. https://doi.org/10.1016/j.joca.2007.03.014.
33. DaSilva JT, Seminowicz DA. Neuroimaging of pain in animal models: a review of recent literature. *Pain Rep*. 2019;4(4), e732. https://doi.org/10.1097/PR9.0000000000000732.
34. Baliki MN, Schnitzer TJ, Bauer WR, Apkarian AV. Brain morphological signatures for chronic pain. *PLoS One*. 2011;6(10), e26010. https://doi.org/10.1371/journal.pone.0026010.
35. Kuner R, Kuner T. Cellular circuits in the brain and their modulation in acute and chronic pain. *Physiol Rev*. 2019;101(1):213–258. https://doi.org/10.1152/physrev.00040.2019.
36. Yezierski RP. The effects of age on pain sensitivity: preclinical studies. *Pain Med*. 2012;13(S2):S27–S36. https://doi.org/10.1111/j.1526-4637.2011.01311.x.
37. Gagliese L, Melzack R. Age differences in nociception and pain behaviours in the rat. *Neurosci Biobehav Rev*. 2000;24(8):843–854. https://doi.org/10.1016/s0149-7634(00)00041-5.
38. Gibson SJ, Farrell M. A review of age differences in the neurophysiology of nociception and the perceptual experience of pain. *Clin J Pain*. 2004;20(4):227–239. https://doi.org/10.1097/00002508-200407000-00004.
39. Ko ML, King MA, Gordon TL, Crisp T. The effects of aging on spinal neurochemistry in the rat. *Brain Res Bull*. 1997;42(2):95–98. https://doi.org/10.1016/s0361-9230(96)00216-x.
40. Boada MD, Gutierrez S, Giffear K, Eisenach JC, Ririe DG. Skin incision-induced receptive field responses of mechanosensitive peripheral neurons are developmentally regulated in the rat. *J Neurophysiol*. 2012;108(4):1122–1129. https://doi.org/10.1152/jn.00399.2012.